

Magnetic Depth Estimation Techniques Applied to the Northern Appalachian Basin

FINAL REPORT

NYSERDA Project 8939-1

Submitted by:

Joseph P. Fagan, Jr., PG
Centennial Geoscience, Inc.
5285 South Perry Court
Littleton, Colorado 80123

For:

Dr. John P. Martin, NYSERDA Project Manager
New York State Energy Research and Development Authority
17 Columbia Circle
Albany, New York 12203-6399

2010

NOTICE

This report was prepared by Centennial Geoscience, Inc. in the course of performing work contracted for and sponsored by the New York State Energy Research and Development Authority (hereafter “NYSERDA”). The opinions expressed in this report do not necessarily reflect those of NYSERDA or the State of New York, and reference to any specific product, service, process, or method does not constitute an implied or expressed recommendation or endorsement of it. Further, NYSERDA, the State of New York, and the contractor make no warranties or representations, expressed or implied, as to the fitness for particular purpose or merchantability of any product, apparatus, or service, or the usefulness, completeness, or accuracy of any processes, methods, or other information contained, described, disclosed, or referred to in this report. NYSERDA, the State of New York, and the contractor make no representation that the use of any product, apparatus, process, method, or other information will not infringe privately owned rights and will assume no liability for any loss, injury, or damage resulting from, or occurring in connection with, the use of information contained, described, disclosed, or referred to in this report.

Introduction

In oil and gas exploration, magnetic methods have been used both to determine the depth to basement in new or unexplored basins and to map positive basement features that affect the depositional patterns of overlying strata (Dobrin and Savit, 1988). Magnetic data are very useful for determining basement structure because the Precambrian has, in most cases, a measurable magnetic response, while the overlying stratigraphic section is mostly non-magnetic. This is due to the presence, or absence, of magnetic minerals in the composition of these rocks. As a result, magnetic surveys can, in many cases, effectively see through the stratigraphic column.

Magnetic responses are created as a result of the magnetic susceptibility of minerals in a body of rock. The susceptibility of a body is a measurement of the degree to which it is magnetized by the earth's field (Nettleton, 1976). Magnetic susceptibility is the critical parameter in magnetic prospecting, just as density is the critical parameter in gravity prospecting. While many minerals possess a measurable magnetic susceptibility, only a few possess significant ones. Of these minerals, the most important is magnetite, while to a lesser extent, pyrrhotite and ilmenite can also be significant. The magnitude of an anomaly is determined by the composition of the causative geologic body. Since different rock types have varying amounts of these magnetic minerals, it follows that certain rock types will display observable magnetic responses while others will not. Table 1 lists the calculated susceptibilities of many common rocks. As can be seen, there is both a great amount of variation for a given type of rock, as well as a significant amount of overlap between different types. However, Table 1 shows that for different types of rocks, there

are recognizable distinctions. For example, basic and ultrabasic igneous rocks usually possess susceptibilities two or three orders of magnitude greater than sedimentary rocks.

Material	Magnetite Content and Susceptibility, cgs units						Ilmenite, average	
	Minimum		Maximum		Average		%	$k \times 10^6$
	%	$k \times 10^6$	%	$k \times 10^6$	%	$k \times 10^6$		
Quartz porphyries	0.0	0	1.4	4,200	0.82	2,500	0.3	410
Rhyolites	0.2	600	1.9	5,700	1.00	3,000	0.45	610
Granites	0.2	600	1.9	5,700	0.90	2,700	0.7	1000
Trachyte-syenites	0.0	0	4.6	14,000	2.04	6,100	0.7	1000
Eruptive nephelites	0.0	0	4.9	15,000	1.51	4,530	1.24	1700
Abyssal nephelites	0.0	0	6.6	20,000	2.71	8,100	0.85	1100
Pyroxenites	0.9	3000	8.4	25,000	3.51	10,500	0.40	5400
Gabbros	0.9	3000	3.9	12,000	2.40	7,200	1.76	2400
Monzonite-latites	1.4	4200	5.6	17,000	3.58	10,700	1.60	2200
Leucite rocks	0.0	0	7.4	22,000	3.27	9,800	1.94	2600
Dacite-quartz-diorite	1.6	4800	8.0	24,000	3.48	10,400	1.94	2600
Andesites	2.6	7800	5.8	17,000	4.50	13,500	1.16	1600
Diorites	1.2	3600	7.4	22,000	3.45	10,400	2.44	4200
Periodotites	1.6	4800	7.2	22,000	4.60	13,800	1.31	1800
Basalts	2.3	6900	8.6	26,000	4.76	14,300	1.91	2600
Diabases	2.3	6900	6.3	19,000	4.35	13,100	2.70	3600

Table 1--Calculated susceptibilities of many common rocks (Dobrin and Savit, 1988)

The susceptibility variations within basement, however, are not the only factors in quantifying magnetic anomalies. In a geologic body, increasing the susceptibility only increases the amplitude of an anomaly. Magnetic anomalies are also dependent upon the strike, dip, depth, and shape of a body. Additionally, the inclination and declination of the earth's field will affect the response (Vacquier et al., 1951). Consequently, by combining these different attributes with available geologic control, it is possible to interpret magnetic fields.

One of the bigger challenges related to the interpretation of magnetic data is the conversion of the data from a measurement of a geophysical property (degree of magnetization) to a direct measurement of the depth to basement. This procedure has undergone several generations of refinement. The first, and simplest, method of conversion of magnetic response to depth to source was based upon profile analysis. These methods, including the slope method and Peter's half-slope method were crude, but effective. The most significant drawback to these methods is that each individual flight line is first printed out on a large scale plotter. Next, each individual anomaly along the length of the profile is analyzed using a ruler and pencil. The depth to the anomaly is calculated using one, or both, of the techniques, and then transferred back to a basemap at the proper location. As a result, the entire process is manual. For a small area, this is not a great drawback. However, as survey size increases, the amount of work quickly grows unwieldy.

As computers became more powerful, many depth estimation techniques were programmed. These automated the process and greatly eased the laborious process discussed above. However, most of these methods still worked on the raw profile data. A three-dimensional, grid-based algorithm was still needed. In the last several years, many different methods were introduced. This paper discusses three of these grid-based techniques: the horizontal gradient (HG) method, the analytic signal (AS) method, and the local wavenumber method. The local wavenumber method is also called the SPI method, and is trademarked by GeoTerrex. These methods were run on a survey that lies

along the basin margin in northern New York. It is along the northern margin of the Adirondack Uplift, in an area called the St. Lawrence Lowlands.

Magnetic processing summary

The following section is intended as a brief summary of the processing of aeromagnetic data. Beginning with the total magnetic field data, several steps must be followed to ensure that the data are ready for interpretation.

Reduction to pole (RTP)

Unlike gravity anomalies that are primarily located over their causative bodies, magnetic anomalies are dependent upon their directions of magnetization and on the direction of the earth's regional field. Reduction to the pole filtering removes the directional dependency of the earth's field and transforms an anomaly into the one that would be observed with vertical magnetization. As a result, reduction to the pole filtering removes asymmetries caused by the non-vertical inducing field and moves the anomalies to a position more directly over their causative bodies, thus facilitating the integration of seismic and gravity data with the magnetic data set. Areas of strong positive anomalies are areas likely containing locally higher susceptibility Precambrian rocks. Similarly, the large, broad magnetic lows are likely areas of lower susceptibility Precambrian rocks. While these broad magnetic highs and lows probably result mostly from lithologic variations in basement, a degree of structural variation may also be present in these anomalies, primarily near the lithologic contacts. It is certain, however, that the biggest anomalies are not caused exclusively by suprabasement features, as the lateral and vertical constraints of such a structure are not supported by other data. The reduction to

the pole operator shifts the larger magnetic responses northwards as much as several thousand feet. Additionally, linear features and contacts are better defined. Instead of selecting a single pair of values for the inclination and declination of both study areas, a continuous reduction to the pole operator was used. This tool allows for the inclination and declination of the magnetic field to be obtained at all places on the grid in a series of map tiles. Each tile is 100 km x 100 km. A 50 km overlap across adjacent tiles exists to allow for cleaner merges when the composite reduced to pole magnetics grid is created.

Horizontal gradient of RTP magnetics

After the reduction to pole correction, a magnetic body is spatially directly associated with the related magnetic response. The maximum gradient of the anomaly slope is located near, or over the body edge. Figure 1 shows a west to east profile over a theoretical magnetic body edge. The magnetic anomaly trace (x-x-x) shows a magnetic high on the positive side of the block and a low on the negative downthrown side. The horizontal gradient operator (□-□-□) computes the absolute value of the slope of the magnetic curve. The maximum of the horizontal gradient curve appears over the contact. That is, the horizontal gradient operator produces maximum ridges on a map over edges of magnetic basement blocks and faults. In addition, the horizontal gradient highlights linear features, related to linear contacts, in the data set. As the horizontal gradient operator enhances high-frequency features, subtle line-oriented anomalies (due to minor “herring-boning”) and small, high-frequency magnetic responses are also enhanced. Because of significant shallow sources, the horizontal gradient tools do not effectively reflect deeper-seated contacts, unless the shallow sources can effectively be removed. The observed magnetic response is a combination of deep crustal sources, basement

lithology variations, structural relief on the basement surface, occasional intrasedimentary sources, and cultural noise.

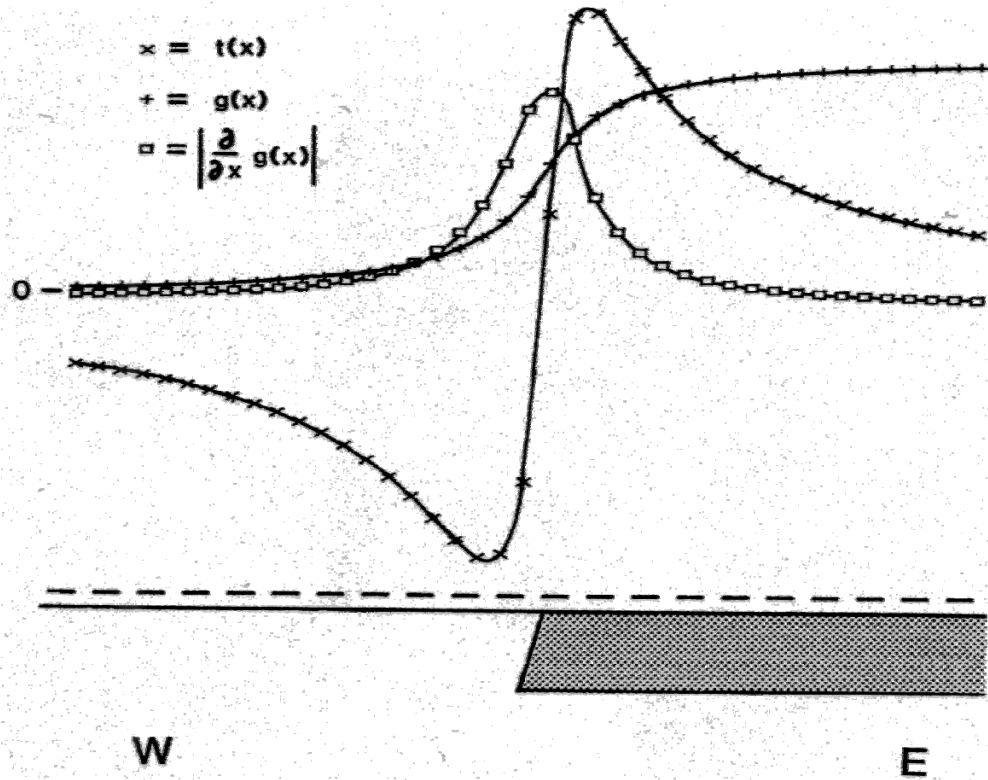


Figure 1—Theoretical magnetic body edge and horizontal gradient (Cordell, 1985)

Each of the above magnetic sources contributes to the entire frequency spectrum, but the depth, lateral extent, and thickness of the individual sources determines into which band of frequencies the body will primarily contribute. Surficial cultural anomalies generally contribute to the highest frequency component, while intrabasement lithology variations contribute primarily to the lowest frequency component. The splitting of the frequency spectrum into components that correspond to basement susceptibility changes, structural discontinuities, and surficial noise is therefore of considerable importance. This splitting is accomplished through Wiener filtering. The frequency spectrum of the survey was

determined, the shallow component was isolated, and the remaining components were mapped.

Vertical gradient of RTP magnetics

Vertical derivatives amplify short-wavelength information at the expense of long-wavelength information. Vertical derivative maps accentuate gradients along edges of shallow magnetic sources. Hence, they can be used to locate edges of magnetic bodies, and to emphasize sources at shallow depths.

Shallow geologic features of limited lateral extent typically have a magnetic anomaly of higher curvature than the regional field (which originates from the deeper sources) on which it is superimposed. The vertical gradient anomaly will be greater over the localized feature than over the more smoothly varying regional trend. Consider, for example, the same magnetic survey sampled at two differing elevations. The broad, low-frequency anomalies that originate from deep within the basement will appear very similar, regardless of whether the field is sampled at 500' or 1,000' above the surface. On the other hand, an anomaly of limited extent will appear significantly different to the two survey elevations. This is because of the relationship between anomaly frequency and the distance the sensor is away from the causative body. The vertical gradient of the magnetic field is the difference in magnetic field responses for the same survey at two different elevations, divided by the difference in flight elevations. In practice, the magnetic field is sampled at only one elevation. By a mathematically stable process known as upward continuation, the magnetic field can be recalculated at a higher elevation. This process requires no knowledge about the actual geometry of the causative

body, or susceptibility distributions. Since both the amount of the upward continuation is known, as is the magnetic responses at the two elevations, it is a straightforward process to calculate the vertical gradient.

Figure 2 shows that by combining the horizontal gradient information, as expressed by the locations of the gradient maxima, with the vertical gradient map, it is possible to determine if the geologic origin of an aeromagnetic anomaly is due to a discrete positive basement feature, a single step function, or two interfering source bodies.

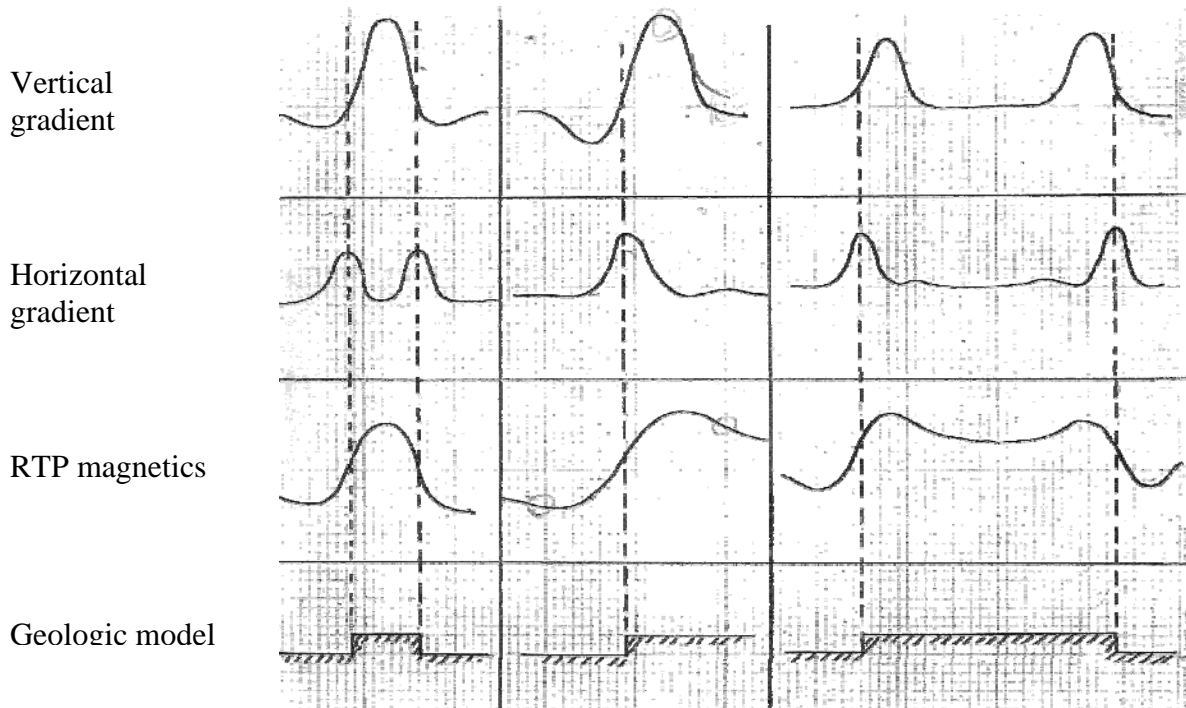


Figure 2—Interpreting geologic structure by combining vertical and horizontal gradients

Summaries of different depth calculation techniques

In order to estimate source depths from gridded aeromagnetic data, it is first necessary to estimate the locations of the magnetic contacts. This is done by constructing a function

from the aeromagnetic data that is peaked over the contacts. Several such functions have been suggested in the literature including the magnitude of the horizontal gradient (Cordell and Grauch, 1982, 1985; Blakely and Simpson, 1986), the amplitude of the analytic signal (Nabighian, 1972; Roest and others, 1992; Roest and Pilkington, 1993), and the local wavenumber (Thurston and Smith, 1997; Smith and others, 1998). In each case, the same function that is used to locate the contacts can be used to estimate the source depths at the contact locations.

Horizontal Gradient Method

The horizontal gradient method is in many ways the simplest approach to estimating contact locations and depths. It requires the greatest number of assumptions about the sources, but is the least susceptible to noise in the data, because it only requires calculation of the two first-order horizontal derivatives of the magnetic field. If $M(x,y)$ is the magnetic field then the horizontal gradient magnitude $HGM(x,y)$ is given by:

$$HGM(x, y) = \sqrt{\left(\frac{\partial M}{\partial x}\right)^2 + \left(\frac{\partial M}{\partial y}\right)^2}$$

This function is peaked over magnetic contacts under the following assumptions: (1) the regional magnetic field is vertical, (2) the source magnetizations are vertical, (3) the contacts are vertical, (4) the contacts are isolated, and (5) the sources are thick. Violations of the first four assumptions can lead to shifts of the peaks away from the contacts. Violations of the fifth assumption can lead to secondary peaks parallel to the contacts.

In order to partially satisfy the first two assumptions, it is usually necessary to perform the standard phase shift operation known as reduction to the pole on the observed magnetic field. Once the field has been reduced to the pole, the regional magnetic field will be vertical and most of the source magnetizations will be vertical, except for sources with strong remanent magnetization such as basic volcanic rocks.

Crests in the horizontal gradient magnitude can be located by passing a small 3 by 3 window over the HGM grid and searching for maxima (Blakely and Simpson, 1986). USGS software from Phillips (1997) uses a similar approach within a 5 by 5 window to both locate the crests and determine their strike direction. Once a crest is located and the strike direction is known, data within the window and within a belt perpendicular to the strike can be used to determine the depth of the contact by performing a least squares fit to the theoretical shape of the HGM over a contact. If h is the horizontal distance to the contact, d is the depth to the top of the contact and K is a constant, then the theoretical curve is given by:

$$HGM(h) = \frac{K}{h^2 + d^2}$$

(Roest and Pilkington, 1993). The least squares fit gives an estimate of both the depth and its standard error, which can be expressed as a percentage of the depth. Typically only depth estimates with standard errors of 15% or better are retained in the final interpretation.

Due to the assumption of thick sources, the depth estimates obtained using the above procedure represent minimum depths. It is also possible to assume very thin sources and

use a standard "pseudogravity" transformation instead of reduction to the pole (Roest and Pilkington, 1993). In this case the same analysis is done on the HGM of the pseudogravity field, and the depth estimates represent maximum depths.

Analytic Signal Method

The function used in the analytic signal method is the analytic signal amplitude of the observed magnetic field, defined by (Roest and others, 1992):

$$A(x, y, z) = \sqrt{\left(\frac{\partial M}{\partial x}\right)^2 + \left(\frac{\partial M}{\partial y}\right)^2 + \left(\frac{\partial M}{\partial z}\right)^2}$$

The analytic signal amplitude peaks over isolated magnetic contacts. As with the horizontal gradient method, the assumption of thick sources leads to minimum depth estimates. Because the analytic signal method requires the computation of the vertical derivative (using Fourier transforms), it is more susceptible to noise than the horizontal gradient method; however, there is no reduction-to-the-pole transformation required.

In a manner identical to that used in the horizontal gradient method, crests in the analytic signal amplitude are located by passing a 5 by 5 window over the grid and searching for maxima. When a crest is found, the local strike direction within the window is determined, and the minimum source depth and its standard error are estimated by a least squares fit to the equation for a two-dimensional analytic signal (Nabighian, 1972):

$$A(h) = \sqrt{\frac{K}{h^2 + d^2}}$$

Local Wavenumber Method

In this method, the function used is the local wavenumber (Thurston and Smith, 1997)

given by:

$$\kappa(x, y, z) = \frac{\left[\frac{\partial^2 F}{\partial x \partial z} \cdot \frac{\partial F}{\partial x} + \frac{\partial^2 F}{\partial y \partial z} \cdot \frac{\partial F}{\partial y} + \frac{\partial^2 F}{\partial z^2} \cdot \frac{\partial F}{\partial z} \right]}{\left[\left(\frac{\partial F}{\partial x} \right)^2 + \left(\frac{\partial F}{\partial y} \right)^2 + \left(\frac{\partial F}{\partial z} \right)^2 \right]}$$

The local wavenumber $\kappa(x, y, z)$ is peaked over isolated contacts. Depths can be estimated without assumptions about the thickness of the source bodies (Smith and others, 1998); therefore the depth estimates may be more accurate than the minimum (or maximum) depths calculated by the other two methods. In addition to the depth, the method yields a parameter called the structural index, which defines the geometry of the source. The edge of a thick body has a structural index of zero. As the thickness of the body decreases, the structural index of the edge moves toward unity. The structural index of a pipe is two; and that of a dipole is three.

Because the local wavenumber requires the calculation of second derivatives, it is very susceptible to noise in the data. It is usually necessary to improve the signal-to-noise ratio of the data either by upward continuation of the aeromagnetic data or the application of a high cut filter prior to calculation of the local wavenumber. In the case of the St. Lawrence Lowlands data, however, neither was applied to the aeromagnetic grid, because of the absence of higher frequencies in the public domain data set.

A computer algorithm similar to the ones used by the other two methods was developed to locate maxima of the local wavenumber within a 5 by 5 window, estimate the local strike direction, and perform a least squares fit to estimate depth and the standard error in the depth.

St. Lawrence Lowlands study area

The area that was examined (Figure 3) as a part of this study was a strip of land along the western and northern margins of the Adirondack Uplift. The strip to the west has been referred to as the St. Lawrence Lowlands, and will be called as such hereafter. While this first study area was chosen for a few reasons, the principal reason was that a previous NYSERDA study was run in 1997. Billman (1999) provided an extensive geologic summary of the area. As such, readers are directed to this report for the stratigraphy and structure of the area. However, a quick summary of the structural geology of the area is appropriate.

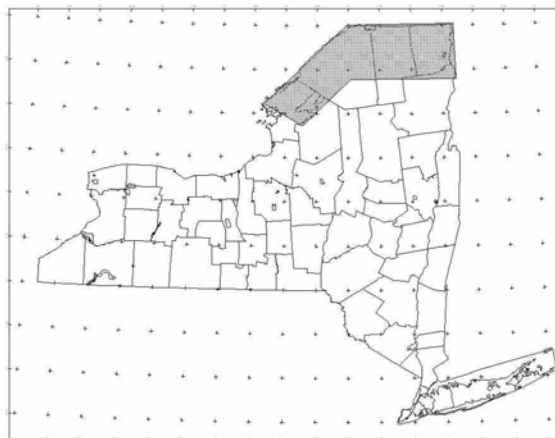


Figure 3—Adirondack Uplift study area

The Potsdam Sandstone was deposited on a fault block Precambrian surface. Sedimentation patterns were affected by this irregular surface. These faults have most likely been reactivated since Cambrian time and have created potential hydrocarbon traps. Flower structures, indicative of strike-slip movement and possible reactivation of these faults, have been documented. This section was later deformed during the Taconic Orogeny, which transformed the extension-dominated tectonic regime into a compressional one. Reactivation of these faults most likely determined the emplacement of lower Ordovician carbonates. Thus, in this area, identifying the location and attitudes of faults is critical in determining the location of both structural and stratigraphic traps. Knowing the depth of the intervening grabens will also be critical in spotting the optimum location for future exploration.

Aeromagnetic data

For this study area, two aeromagnetic surveys that were flown in the 1970s were used. The data are in the public domain data, and are available from NOAA. Figure 4 is a map of the total magnetic intensity data. Several features are easily observable on the total magnetic intensity map. First, the overall frequency content of the data set is higher than typical for many public domain data sets. This is due to two factors: (1) the shallow depth to basement, and (2) the relatively narrow spacing of the flight lines (800 m). Second, there are both large positive and negative magnetic anomalies. This is due to the significant variety of lithologies present in the Adirondacks. Third, the predominant grain observed trends NE-SW. This trend is reflected in both the edge of the Adirondack Uplift and the St. Lawrence River, whose location is fault controlled.

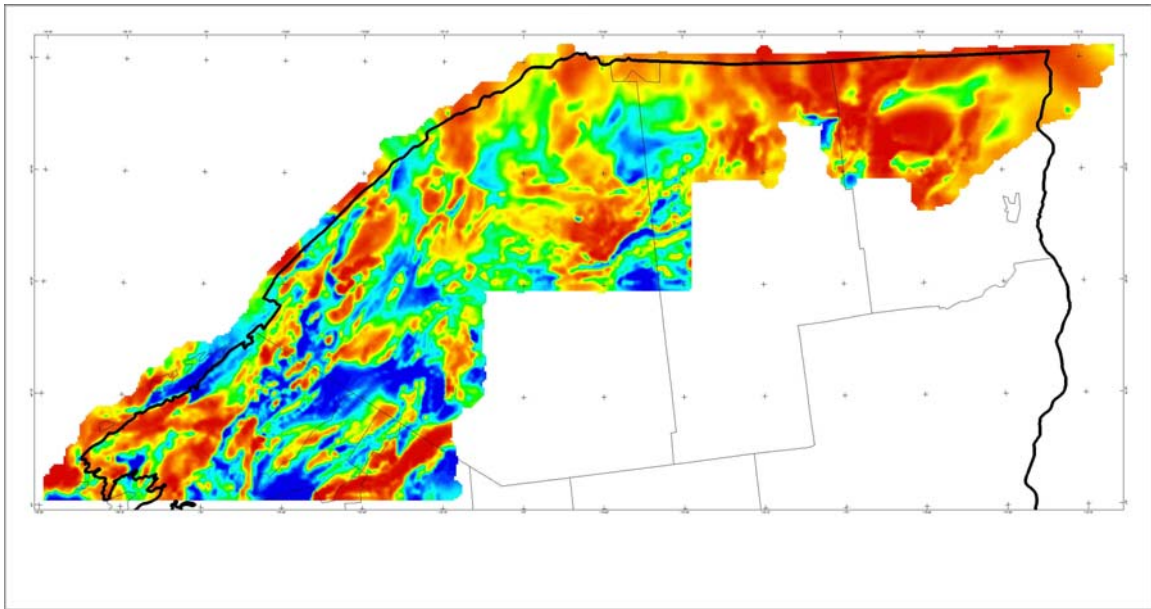


Figure 4—Total magnetic intensity map of Adirondack Uplift study area

Following the aeromagnetic processing procedure outlined beginning on page four, several data sets were created for analysis. The first of these is the reduced to pole total magnetic intensity, or RTP. Figure 5 shows the effect of removing the earth's magnetic field from the survey. The average geomagnetic inclination in the study area is 73.5° . After application of the operator, the magnetic anomalies have been repositioned approximately one kilometer to the north. The average geomagnetic declination of the earth's field, -13.3° , does not significantly affect this area. Hence, there is only a very small "twisting" of the anomalies after the reduction to pole operator is applied. In some instances, a small high-cut filter is simultaneously applied to the data set during the reduction to the pole operation. This is typically done in lower magnetic latitudes, where the operation can cause the amplitude and frequency of anomalies to increase significantly. However, in this area, no high cut filter was applied, as there is no indication of this type of filter singularity problem.

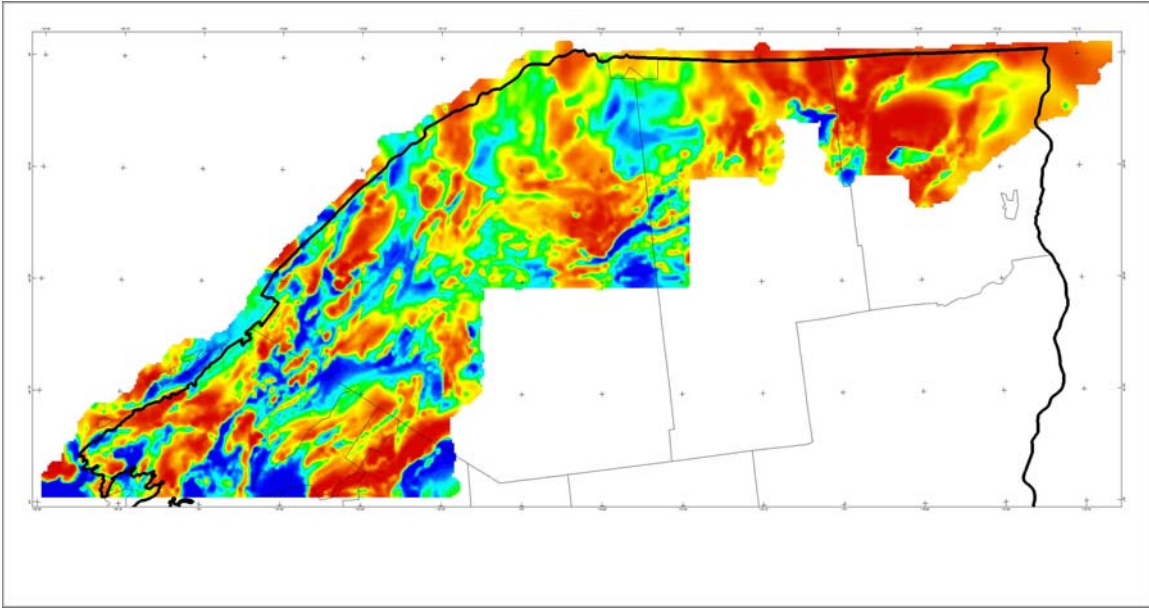


Figure 5—Reduced to pole total magnetic (RTP) map of Adirondack Uplift study area

The horizontal gradient of the RTP magnetics reflects the observations listed above. First, the dominant NE-SW grain of the data is easily visible. Also, the high-frequency component of the data is evident. Figure 6a shows the horizontal gradient displayed as a shaded relief image. In this image, the inclination of the light source is 45° , and its declination is 315° . Figure 6b shows the horizontal gradient as a color map. This data set provides the function that is the basis of the first depth estimation algorithm.

The horizontal gradient function is part of the analytic signal. Recalling that the horizontal gradient is the square root of the sum of the squares of the partial derivatives,

$\frac{\partial F}{\partial x}$ and $\frac{\partial F}{\partial y}$, and that the third component in the function is just the vertical

derivative, $\frac{\partial F}{\partial z}$, it is necessary only to figure it to also obtain the analytic signal. This is

important, as this function is used in the second depth estimation algorithm.

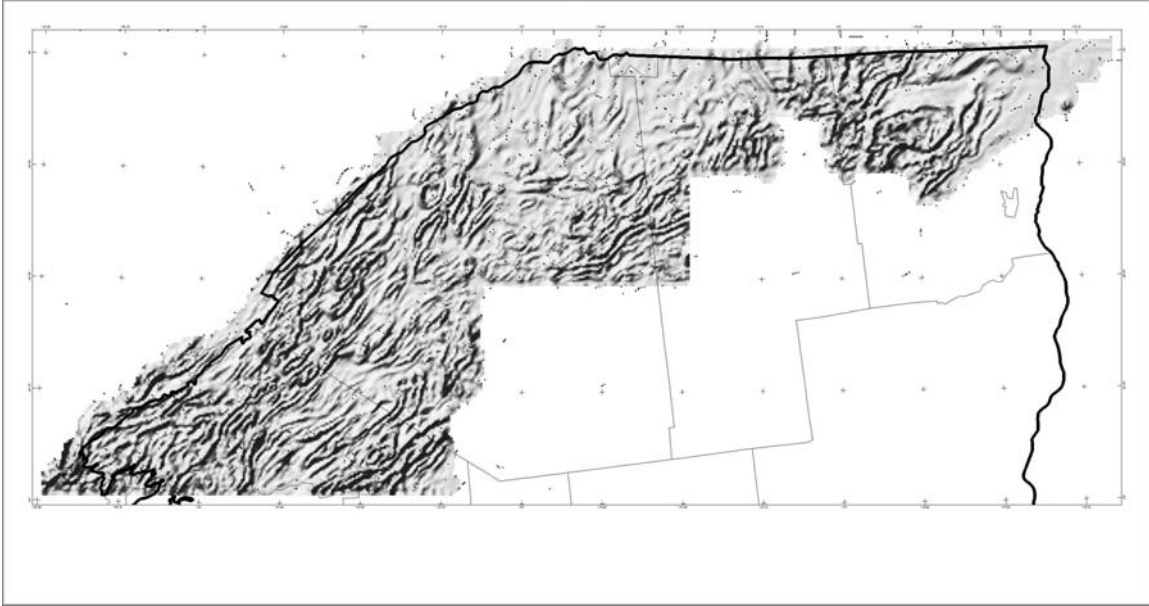


Figure 6a—Shaded relief image of horizontal gradient of RTP magnetics

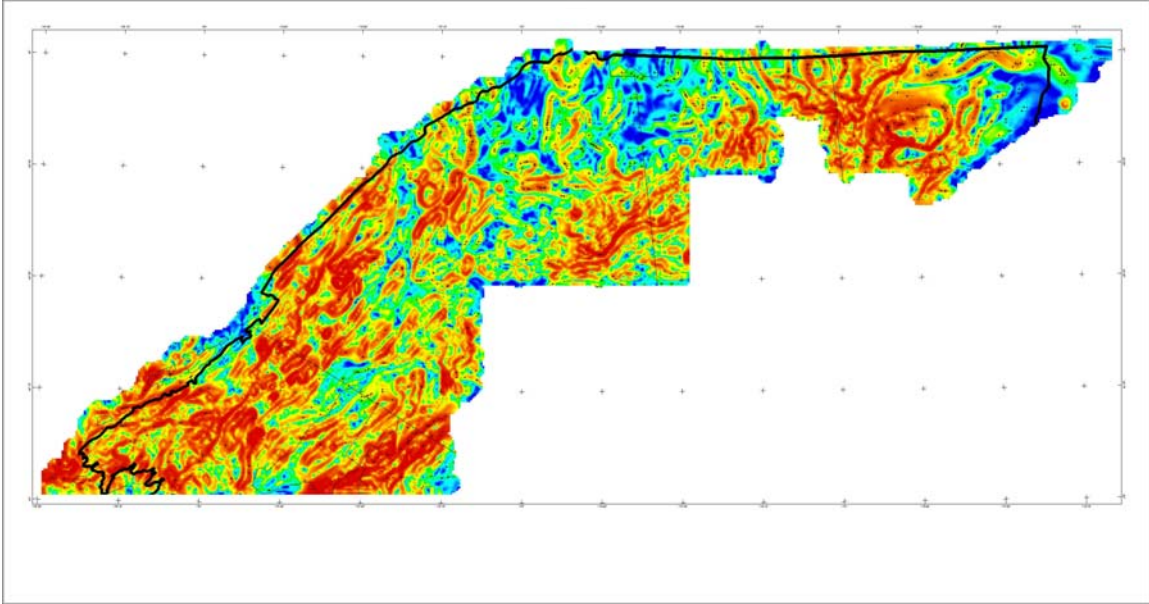


Figure 6b—Color image of horizontal gradient of RTP magnetics. This grid serves as the input function to the first depth estimation algorithm.

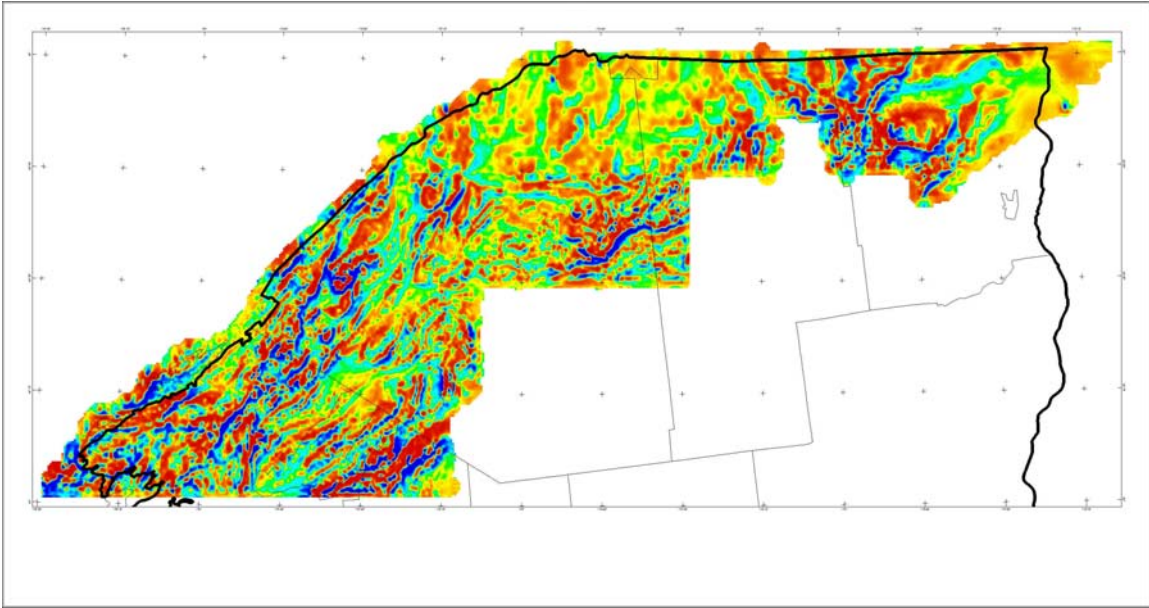


Figure 7—Vertical derivative of reduced to pole magnetics

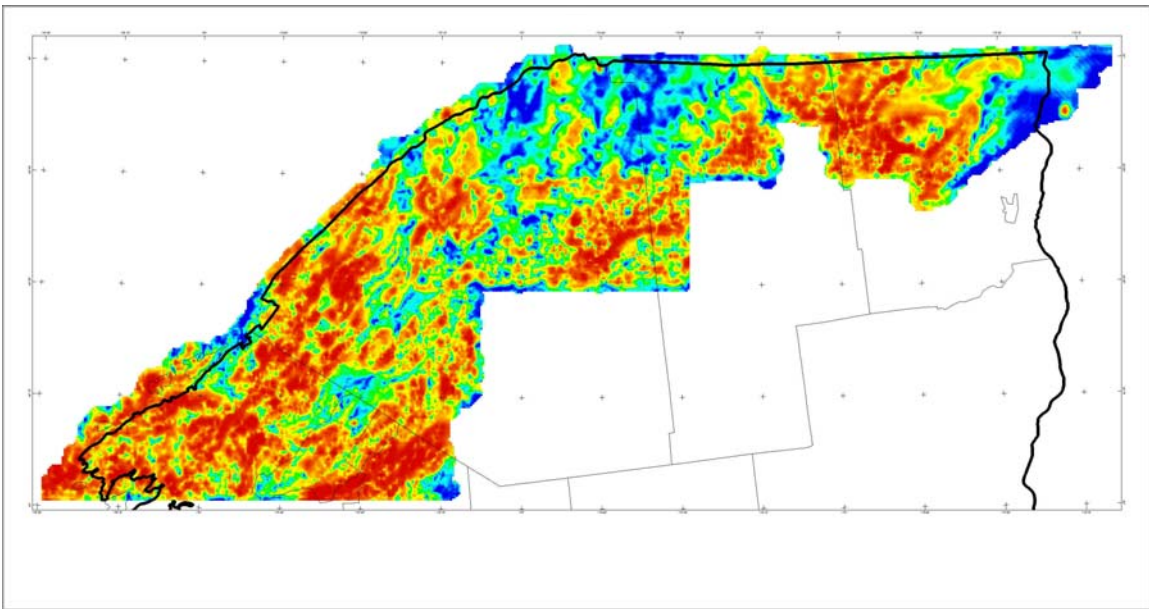


Figure 8—Analytic signal of reduced to pole magnetics

Figure 7 shows the vertical gradient of the RTP magnetics. The vertical gradient is often a very noisy appearing map. This is due to the fact that, as previously mentioned, higher frequency anomalies are accentuated, while lower frequencies are suppressed. As a result of this, localized anomalies that are either highly negative or positive are often observed next to anomalies of opposite magnitude. Discontinuities in the data set are accentuated as well. As a result, a high cut filter is often applied to the vertical derivative data set to boost the signal-to-noise ratio. For this study area, a high-cut Butterworth filter centered on 3,000 meters was applied.

Figure 8 is a map of the analytic signal. The analytic signal is calculated using the Hilbert transform. Local peaks in the analytic signal profile are interpreted as corners of source bodies and the shape of the peak contains information about the depth to the corner. In the absence of high-frequency noise and aliasing in the data, horizontal locations from analytic signal are highly accurate. Again, the grid in Figure 8 served as the input for the second depth estimation technique.

By combining a variety of first and second derivatives (both horizontal and vertical), the local wavenumber grid is created. Figure 9 shows the variation of this grid, identified by the Greek letter κ , as defined above on page 12. It should be noted that while the general shape of anomalies observed on the local wavenumber grid is similar to those in both the horizontal gradient grid and analytic signal grid, the amplitudes of the grids are very different. This is due to the fact that the local wavenumber grid incorporates higher order derivatives in the computation.

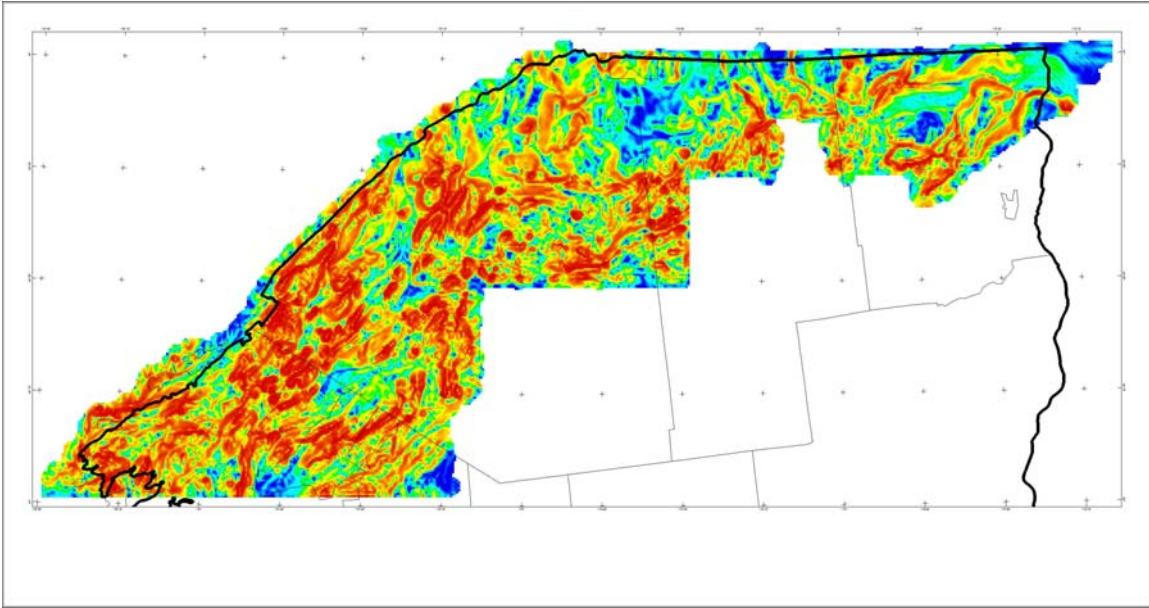


Figure 9—Local wavenumber function, κ , from reduced to pole magnetics

Depth calculation results

The first observation from comparing the three different methods (Figures 10, 11, and 12) is that the results are relatively similar between all three methods. This is especially true in comparing the horizontal gradient and analytic signal methods. This result is not surprising, considering the formulae that are used to calculate these responses.

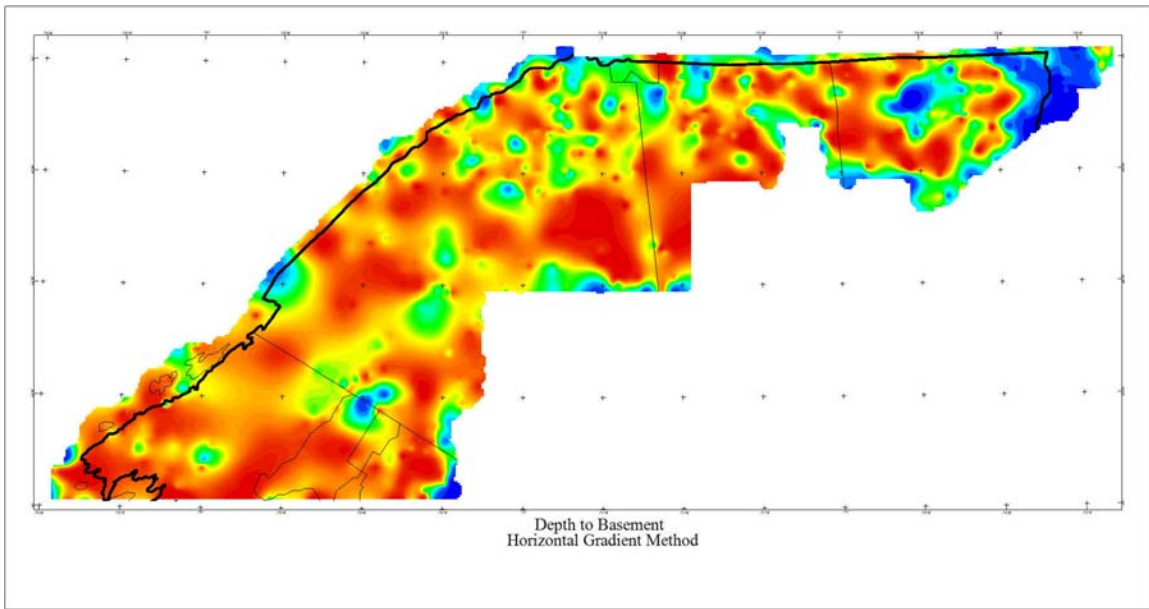


Figure 10—Depth to basement from HG method (red=shallow; blue=deep)

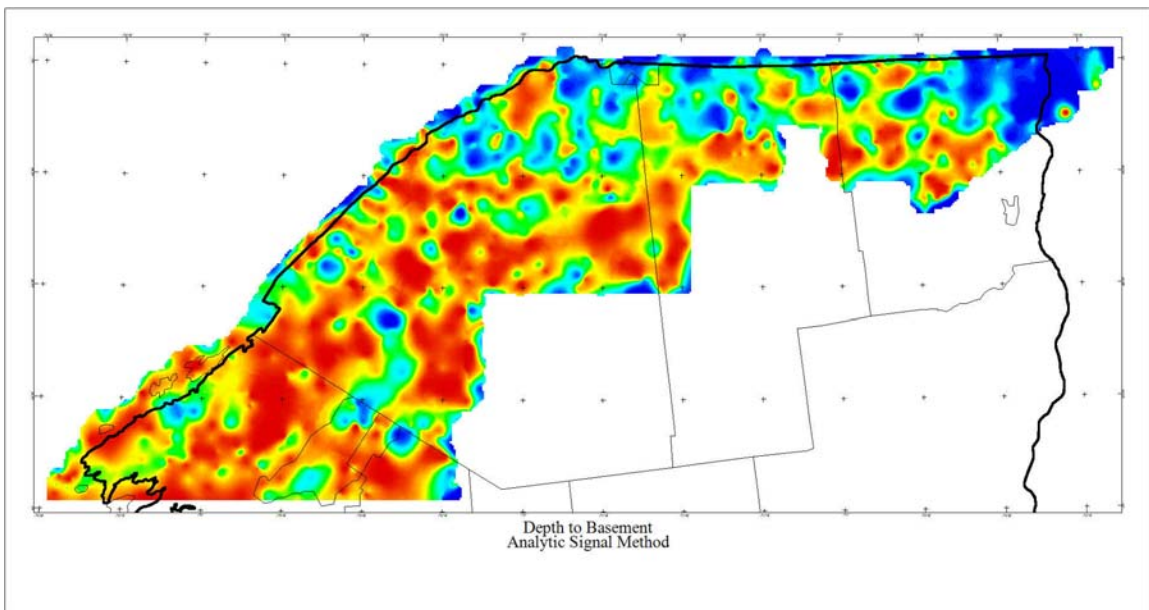


Figure 11—Depth to basement from AS method (red=shallow; blue=deep)

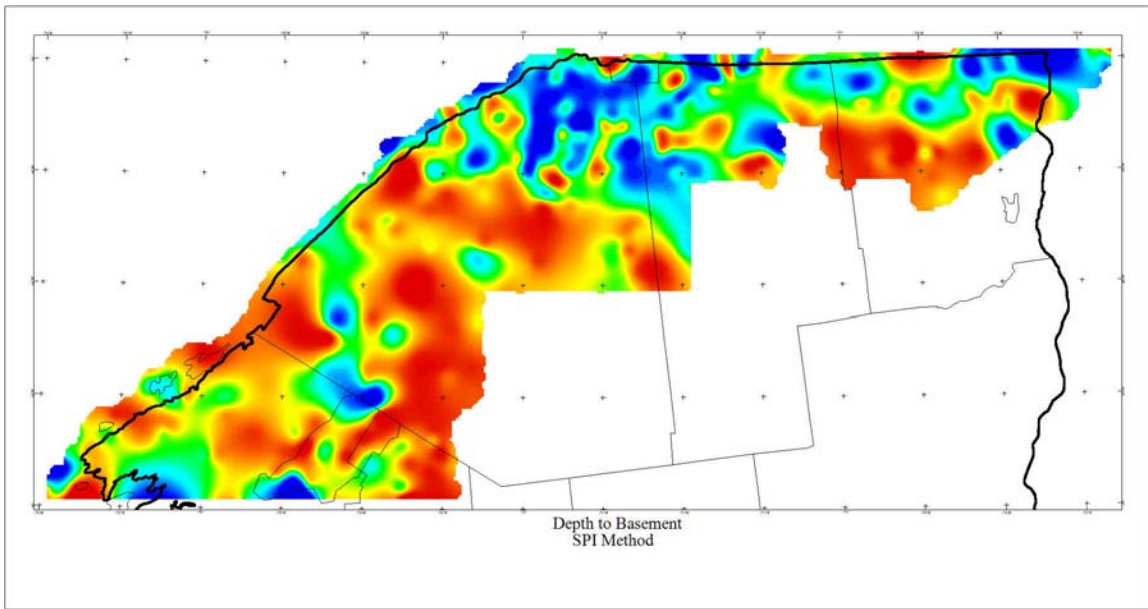


Figure 12—Depth to basement from SPI method (red=shallow; blue=deep)

The analytic signal method has more high frequency features in the observed data. As mentioned above, this is due to the presence of the vertical gradient, $\frac{\partial F}{\partial z}$, in the depth calculation. In the display of the SPI method results (Figure 12), it was necessary to apply a high-cut filter to the display. The higher order derivatives make the image very discontinuous. All three methods show that the depth to basement is very shallow in the southwestern portion of the survey. This corresponds with the Frontenac Arch. However, the HG method shows a more continuous high area just north of the Jefferson/St. Lawrence county boundary. Both the AS and SPI methods show that there is a low that trends approximately N-S.

All three methods indicate that the depth to basement increases from south to north. This agrees with the general geology of the area. The thickness of stratigraphic cover increases off of the flanks of the Adirondack Mountains. Additionally, the St. Lawrence River

follows an older rift system. Both of these factors account for the greater depths observed on the maps.

Near the eastern edge of the survey, along the New York/Vermont boundary, all three methods indicate that the depth to basement increases, perhaps significantly. The Lake Champlain-Lake George region shows several surficial faults. In all likelihood, these basement faults have been reactivated throughout geologic time. Of the three methods, only the SPI method indicates that this graben is not one continuous feature.

Conclusions

All three of the magnetic depth estimation techniques have yielded reasonable results. The primary advantage of the SPI method lies in the flexibility of designating the structural index parameter. This method allows individual types of anomalies to be modeled quickly. Using any magnetic depth estimation technique, it is possible to calculate depths to individual anomalies to $\pm 20\%$. This process can be time consuming, however. In most cases, the *absolute* depth to basement is not as important as the *relative* depth to basement. The techniques used in this paper can quickly delineate areas that are structurally higher or lower. In the case of the St. Lawrence Lowlands area, locally high blocks in areas that have a greater depth to basement may reflect the tops of uplifted horst blocks as described by Billman (1999). The edges of these highs may serve as areas of structural trapping; in these areas, the Potsdam Ss. and the Beekmantown Group may

exhibit flexure and pinch-out traps. Also, these areas may be loci for traps related to strike-slip motion traps, as are seen across the border in Quebec.

These techniques can quickly analyze an area of several counties at one time. An area the size of this study area can be pre-processed for the depth estimation techniques in under an hour. The actual depth estimation can be done in a few hours, thereby quickly yielding a good first-approximation to the configuration of the basin. This should allow further exploration techniques to be focused optimally, thereby reducing the cost of exploration.

References

Billman, D., 1999, Hydrocarbon Potential in the St. Lawrence Lowlands of Northern New York, NYSERDA Study [4550-ERTER-ER-97](#)

Blakely, R.J., and Simpson, R.W., 1986, Approximating edges of source bodies from magnetic or gravity anomalies: *Geophysics*, v.51, no.7, p.1494-1498.

Cordell, Lindrith, and Grauch, V.J.S., 1982, Mapping basement magnetization zones from aeromagnetic data in the San Juan Basin, New Mexico: Society of Exploration Geophysicists, 52nd Annual Meeting, Abstracts and Bibliographies, p.246-247.

Cordell, Lindrith, and Grauch, V.J.S., 1985, Mapping basement magnetization zones from aeromagnetic data in the San Juan basin, New Mexico *in* Hinze, W.J., ed., The utility of regional gravity and magnetic anomaly maps: Society of Exploration Geophysicists, p.181-197.

Dobrin and Savit, *Introduction to Geophysical Prospecting*.. New York-London: McGraw-Hill, 1952. 435 pp.

Nabighian, M.N., 1972, The analytic signal of two-dimensional magnetic bodies with polygonal cross-section: its properties and use for automated anomaly interpretation: *Geophysics*, v.37, no.3, p.507-517.

Nettleton, L.L., *Gravity and magnetics in oil prospecting*, McGraw-Hill, 464 pp., 1976.

Phillips, J.D., 1997, Potential-field geophysical software for the PC, version 2.2: U.S. Geological Survey Open-File Report 97-725, 34p.

Roest, W.R., and Pilkington, Mark, 1993, Identifying remanant magnetization effects in magnetic data: *Geophysics*, v.58, no.5, p.653-659.

Roest,W.R., Verhoef, Jacob, and Pilkington, Mark, 1992, Magnetic interpretation using the 3-D analytic signal: *Geophysics*, v.57, no.1, p.116-125.

Smith, R.S., Thurston, J.B., Dai, Ting-Fan, and MacLeod, I.N., 1998, iSPItm - the improved source parameter imaging method: *Geophysical Prospecting*, v.46, p.141-151.

Thurston, J.B., and Smith, R.S., 1997, Automatic conversion of magnetic data to depth, dip, and susceptibility contrast using the SPItm method: *Geophysics*, v.62, no.3, p.807-813

Vacquier, V., Steenland, N. C., Henderson, R. G. and Zeitz, I., Interpretation of eromagnetic maps. *Geol. Soc. Am. Mem .*, 1951, 47, 151.